# Seismic performance assessment of a pile-supported wharf retrofitted with different slope strengthening strategies

**Lei Su[1], Hua-Ping Wan[2*], Yaozhi Luo[2], You Dong[3], Jinchi Lu[4], Xian-Zhang Ling[1], Ahmed Elgamal[4], Arul K. Arulmoli[5]**

*[1]School of Civil Engineering, Qingdao University of Technology, Qingdao, China*
*[2]Department of Civil Engineering, Zhejiang University, Hangzhou, China*
*[3]Department of Civil and Environmental Engineering, The Hong Kong Polytechnic University, Kowloon, Hong Kong*
*[4]Department of Structural Engineering, University of California, San Diego, USA*
*[5]Earth Mechanics Inc., California, USA*

## Abstract

Pile-supported wharves may be subjected to severe damage during major earthquakes. As such, efficient strategies for retrofitting wharf systems are needed. In this study, we investigate the seismic performance of a pile-supported wharf retrofitted by the following three conventional slope strengthening strategies: i) improving the ground with a soil-cement mixture, ii) driving pin piles near dike toe, and iii) creating an underwater bulkhead system using sheet piles. Effectiveness of the three retrofit schemes is assessed comprehensively. First, seismic response of the as-built and retrofitted pile-supported wharf is investigated. Subsequently, performance of the retrofit strategies in mitigating the seismic vulnerability is thoroughly investigated by comparing component- and system-level fragility curves. It was found that: (1) overall, the strategies are effective in mitigating the seismic response and in reducing the seismic fragilities of the wharf system; (2) the performance of the retrofit measures varies at the structural component level, as a retrofit measure may have an isolated local negative effect for a certain structural component. In this regard, an appropriate retrofit strategy should be identified based on specifically defined retrofit purposes; and (3) as implemented, the soil-cement mixture performed best (in lowering the system seismic fragility), followed by the pin pile, and lastly the sheet pile.

**KEYWORDS:** Seismic performance, Pile-supported wharf; Retrofit; Slope improvement; Fragility analysis; Soil-pile interaction.

## Introduction

In general, a pile-supported wharf usually involves one or more berths, and also consists of pile foundation, deck, and other necessary facilities for supporting the containers. Pile-supported wharves, which accommodate import and export activities, are a critical component of the transportation and utility networks. As the commercial and industrial activities in national as well as international scale increasingly depend on trade, pile-supported wharves and seaport systems play an important role in maintaining the welfare of the general public, protecting significant capital investments, and promoting national prosperity. As a result, operational

*Corresponding author.
*E-mail address*: sulei@qut.edu.cn (L. Su); hpwan@zju.edu.cn (H.-P. Wan); luoyz@zju.edu.cn (Y. Luo); you.dong@polyu.edu.hk (Y. Dong); jinlu@ucsd.edu (J. Lu); lingxianzhang@qut.edu.cn (X.-Z. Ling); elgamal@ucsd.edu (A. Elgamal); Arulmoli@earthmech.com (K. Arulmoli)

failure and damage will cause substantial economic loss, including the direct repair cost and indirect business disruption owing to the resultant service interruption of the port system.

Many pile-supported wharves located in seismically active regions are particularly vulnerable to seismic hazard. Post-earthquake field observations have demonstrated that pile-supported wharves were frequently subjected to extensive damage during major earthquakes, such as the 1989 Loma Prieta [1], the 1995 Hyogoken-Nanbu earthquake [2], and the 2010 Haiti earthquake [3], among others.

Many existing infrastructure systems (such as, bridges, building, and wharves) may not have adequate seismic resistance as required by the current codes and guidelines partially because they were built prior to current earthquake resistant design codes [4, 5]. In addition, pile-supported wharves are continuously deteriorating over the course of service life due to a variety of factors, including but not limited to cargo volume growth, corrosion, and harsh environment attacks. In this respect, the as-built pile-supported wharves designed without adequate seismic detailing or in a seismic region with an increased hazard level are more susceptible to damage during an earthquake event.

Demolition and reconstruction of such seismically deficient pile-supported wharves is not an easy task and also requires much time and money. On the other hand, retrofit and strengthening of these as-built wharves could be more convenient and cost-effective to improve their seismic performance and to help mitigate their functionality loss. This highlights the importance of comprehensive seismic performance assessment of pile-supported wharves with different retrofit measures, aiming to quantify the effectiveness of various seismic retrofit measures for wharf structures and to prioritize an optimal retrofit strategy.

The significance of seismic performance of the retrofitted infrastructure systems has been increasingly recognized among the earthquake engineering community, and in response, a surge of work has been done in this research branch. In the literature, most studies are concerned with seismic retrofit of bridges (see e.g., [6-17]). The seismic retrofit and strengthening solutions adopted in practical applications for bridges mainly include (1) improving the ductility, shear strength of bridge columns, cap beams and bents, as well as offering confinement by jacking or wrapping the columns using either traditional or advanced materials; (2) reducing the demands that earthquakes place on bridges by incorporating seismic isolation bearings and damping devices; and (3) limiting excessive motions to mitigate potential pounding and unseating by cable or bar restrainers. Kim and Shinozuka [6] carried out a nonlinear dynamic analysis of bridges before and after column retrofit with steel jacketing, and evaluated the improvement in the fragility with steel jacketing by comparing fragility curves of the bridge with and without seismic retrofit. Casciati et al. [7] explored the seismic reliability of a retrofitted cable-stayed bridge installed with hysteretic damping devices in terms of fragility curves. Padgett and DesRoches [8, 9] developed fragility curves for retrofitted bridges and also assessed the influence of various retrofit measures on component and system seismic vulnerability. Zhang and Huo [10] and Xie and Zhang [11] conducted the seismic performance assessment of highway bridges equipped with seismic isolation devices and investigated the optimum design of isolation devices as well. Billah et al. [12, 13] carried out seismic performance evaluation of multi-column bridge bents retrofitted with four different retrofit techniques using either fragility analysis or incremental dynamic analysis. Zakeri et al. [14] evaluated the effects of versatile retrofit strategies on seismic performance of skewed bridges in terms of fragility curves. DesRoches and Delemont [15] evaluated the efficacy of using shape memory alloy (SMA) restrainers for seismic retrofit of a typical multi-span simply supported bridge through a comparison with the conventional steel restrainer cables.

Zheng et al. [16] fully assessed the effect of SMA-cable-based novel bearing on the bridge seismic performance in terms of vulnerability, loss, resilience, and life-cycle loss. Abbasi and Moustafa [17] conducted a probabilistic seismic assessment of older and newly-designed reinforced concrete bridges based on system and component fragility curves under different damage states. In addition to bridges, seismic retrofit of buildings also has captured significant attention. The representative research work can be found in [18-20].

Although seismic performance of as-built pile-supported wharves has been increasingly investigated [21-34], little work has been done to date on retrofitting of existing pile-supported wharves or evaluating the effectiveness of various retrofit measures on seismic performance. To the best of the authors' knowledge, only two studies have investigated the seismic performance of retrofitted pile-supported wharves [5, 35]. In contrast to bridges and buildings, which are mostly onshore structures, the pile-supported wharves are waterfront facilities directly exposed to the marine environment. Considering this unique operational condition, some widely-used retrofit strategies for bridges and buildings, such as energy dissipation devices, wire pre-stressing, and steel jacking, may be not easily implementable or not appropriate for retrofitting of pile-supported wharves. As such, there is a strong need for designing multiple rehabilitation techniques that are practical for improvement of the as-built pile-supported wharves, and fully investigating the comparative seismic performance of these target retrofit measures to prioritize the most effective ones.

In this study, a typical pile-supported wharf structure is considered. The target pile-supported wharf consists of 6 rows of pre-stressed concrete piles, almost all of which are on a dike with an inclination of 31 degrees (noting that stability of the dike is very important for safeguarding this wharf-ground system against seismic hazard). In this regard, the aim of seismic retrofit of this pile-supported wharf is to improve the slope stability of the dike. Three practical retrofit measures, that is, creating a soil-cement mixture near the dike toe, driving pin piles, and constructing a sheet pile wall at the dike toe, are considered for seismic retrofit. Both deterministic and probabilistic seismic analyses are utilized to evaluate the effectiveness of these three seismic retrofit measures. For deterministic seismic analysis, a wide spectrum of seismic responses (e.g., displacements of wharf deck and slope, bending moments of piles, and deformation of the whole wharf system) before and after retrofit are fully explored under a representative seismic excitation scenario. On the other hand, for the probabilistic seismic analysis, the record-to-record variability of ground motions is taken into account in the seismic performance assessment. A suite of 80 ground motions extracted from the Pacific Earthquake Engineering Research Center Strong Motion Database are selected to perform nonlinear time history analysis. On this basis, the effectiveness of different slope strengthening strategies is thoroughly investigated by fragility analysis at both component- and system-levels.

To summarize, the main contributions of this work are threefold. First, three different slope strengthening strategies are introduced for retrofitting of a large-scale pile-supported wharf. Second, numerical modeling of the as-built and retrofitted wharf structures is detailed. A nonlinear FE model is developed for dynamic analysis of a fully coupled wharf-ground system. In particular, a soil-water fully coupled formulation is employed with a soil constitutive model via a multi-surface plasticity framework. Third, the retrofit effectiveness of three different slope strengthening strategies on pile-supported wharf is comprehensively assessed in terms of deterministic and probabilistic seismic analyses. Especially for the probabilistic seismic analysis, the performance of different slope strengthening strategies is thoroughly evaluated by fragility analysis at both component- and system-levels.

## As-Built Pile-Supported Wharf and Retrofit Strategies

### Description of as-built pile-supported wharf

As shown in Fig. 1, a wharf-ground configuration derived from the Port of Los Angeles Berth 100 layout [36] is considered. This target wharf structure is 317 m long in the longitudinal direction and 30.5 m wide in the transverse direction (Fig. 2a). Along the longitudinal direction, there are 52 bays arranged equally at a spacing of 6.1 m, and along the transverse direction, there are 6 rows of pre-stressed reinforced concrete piles. The distance between the pile rows E and F is 3.7 m, whereas the distance among the remaining pile rows is 6.7 m (Fig. 2b). Below ground lengths of the pile rows E and F are identical while the below ground lengths of pile rows A-D are varying. The reinforced concrete piles, each being 42 m long, are composed of the core and cover concretes, and strands enclosed with spiral reinforcement (Fig. 2c), and their cross-sections are of octagonal shape whose sides are 0.253 m (Fig. 2d). The concrete deck supported on these reinforced concrete piles is at least 0.4 m thick. The dike, aiming to enhance the stability of this large-scale wharf structure, has an inclination of 31 degrees. On the landside, there are 8 soil layers, comprising 3 soil types (i.e., marine sand, lagoonal clay, and lakewood-San Pedro sand), while on the waterside, there are 4 soil layers only. The dike slope is covered by the quarry run. Properties of these soil layers are presented in Table 1.

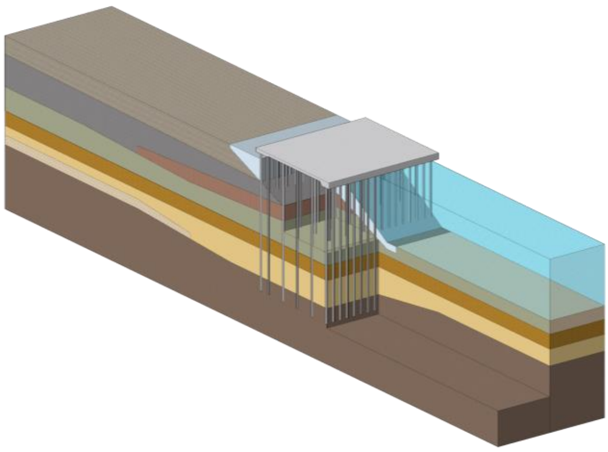

**Figure 1. Three-dimensional view of pile-supported wharf structure.**

### Details of retrofitting strategies

Due to presence of the weak clay stratum with low shear modulus and cohesion (soil layer IIIA in Table 1) below the dike section, the safety reserve of the dike section against seismic failure may not be adequate, especially when subjected to strong dynamic loadings (e.g., large seismic events). Su et al. [32] reported that such a weak clay stratum will amplify the seismic shear deformation, which leads to large seismic deformation of the soil and wharf structure above this layer, especially within the dike layer. Therefore, the retrofit strategies are concerned with slope improvement for the dike.

Three retrofit techniques are considered to strengthen the slope toe zone and mitigate excessive slope deformations [36]. A schematic of these retrofit strategies is shown in Fig. 3. The first retrofit strategy (Fig. 3a) is the soil-cement mixture ground improvement scheme, which seeks to increase the shear resistance of the clay layer below the dike section so as to improve slope stability by mixing cement with the soil and creating a soil-cement mixture. The retrofit zone is 19.2 m long, 10.4 m high on the landside, and 8.4 m high on the waterside. The shear modulus of the soil-cement mixture is taken as 524 MPa and its cohesion is 498 kPa, which are determined according to [37, 38]. The second retrofit strategy (Fig. 3b) consists of driving pin piles near the dike toe. The center-to-center spacing of the pin piles ranges from 1.7 m to 3.0 m and their lengths range from 8.5 m to 13.9 m. A total of 10 pin piles with an inside radius of 187 mm and an outside radius of 190.5 mm are installed. The flexural stiffness of pin piles is set to $5.26\times10^4$ kN-m$^2$ adopted from [39]. The third retrofit strategy (Fig. 3c) employs an underwater bulkhead system consisting of sheet piles. Steel sheet piles are long structural sections with a vertical interlocking mechanism that creates a continuous wall that is most often used to retain either soil or water. The sheet piles are Z-shaped and their detailed dimensions are shown in Fig. 3(c). Lengths of sheet piles are 9.0 m and their base elevation is the same as that of the wharf piles.

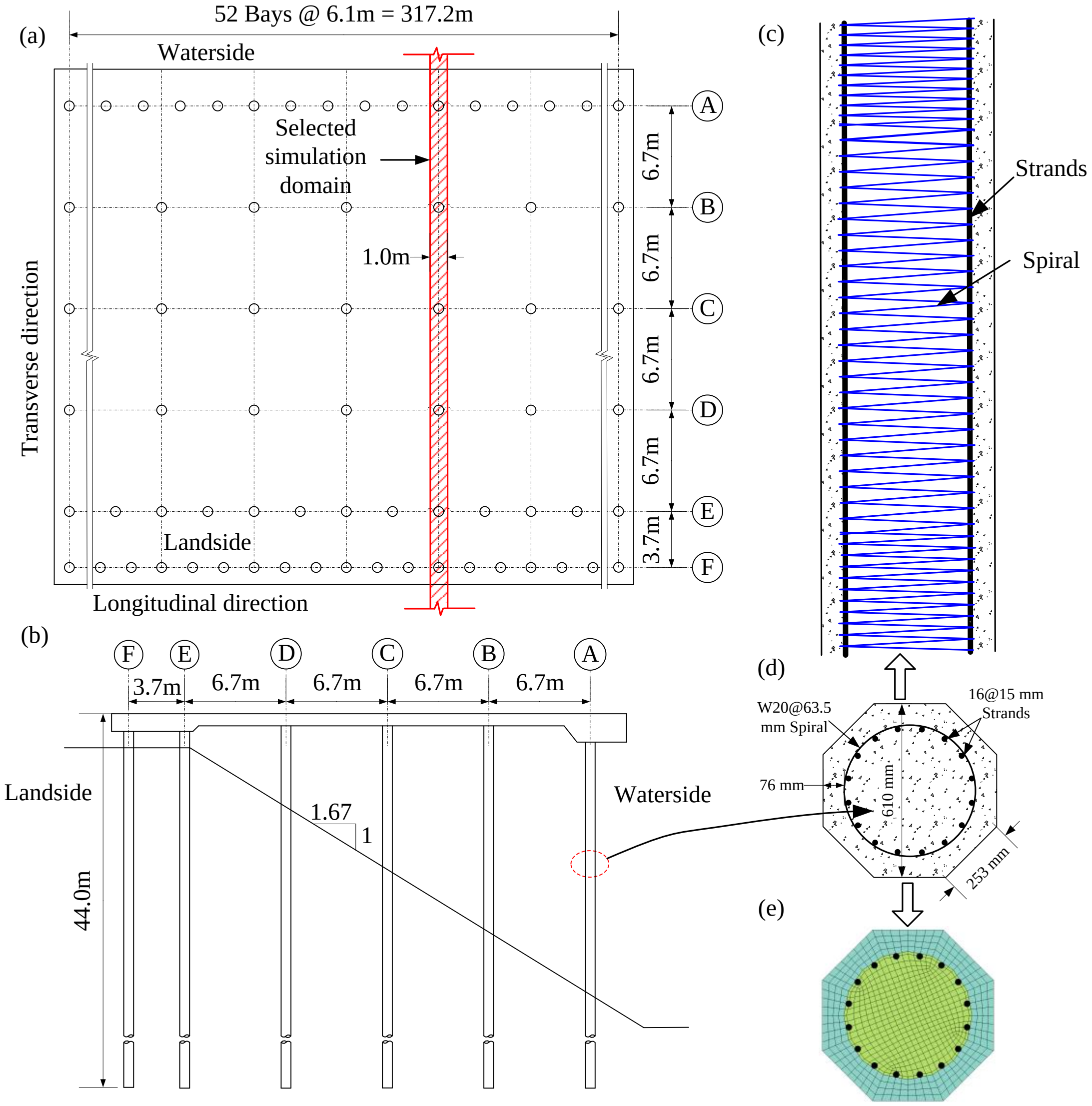


**Figure 2. Configuration of wharf structure: (a) Wharf plan; (b) Wharf elevation; (c) Pile elevation; (d) Cross-section of pile; (e) Fiber section of pile.**

**Table 1. Physical properties of soil under wharf structure [32].**

| Soil unit | | Soil description | Density, $\rho$ (kg/m$^3$) | Friction angle, $\varphi$ (°) | Shear modulus, $G$ (MPa) | Bulk modulus, $B$ (MPa) | Cohesion, $c$ (kPa) |
|---|---|---|---|---|---|---|---|
| I | | Sandy fill (above ground water table) | 1920 | | | | |
| II | A | Loose marine sand | 1920 | 32 | 100 | 469 | 0 |
| | B | Dense marine sand | 2000 | 36 | 151 | 703 | 0 |
| | C | Medium dense marine sand | 2000 | 34 | 127 | 591 | 0 |
| III | A | Soft to stiff lagoonal clay | 1760 | 0 | 26 | 122 | 80 |
| | B1 | Stiff lagoonal clay | 1840 | 0 | 43 | 200 | 108 |
| | B2 | Stiff lagoonal clay | 1840 | 0 | 84 | 391 | 135 |
| IV | A | Dense lakewood-San Pedro sand | 2000 | 36 | 186 | 868 | 0 |
| | B | Very dense lakewood-San Pedro sand | 2080 | 38 | 279 | 1300 | 0 |
| - | Dike | Quarry run | 2240 | 45 | 141 | 1363 | 20 |

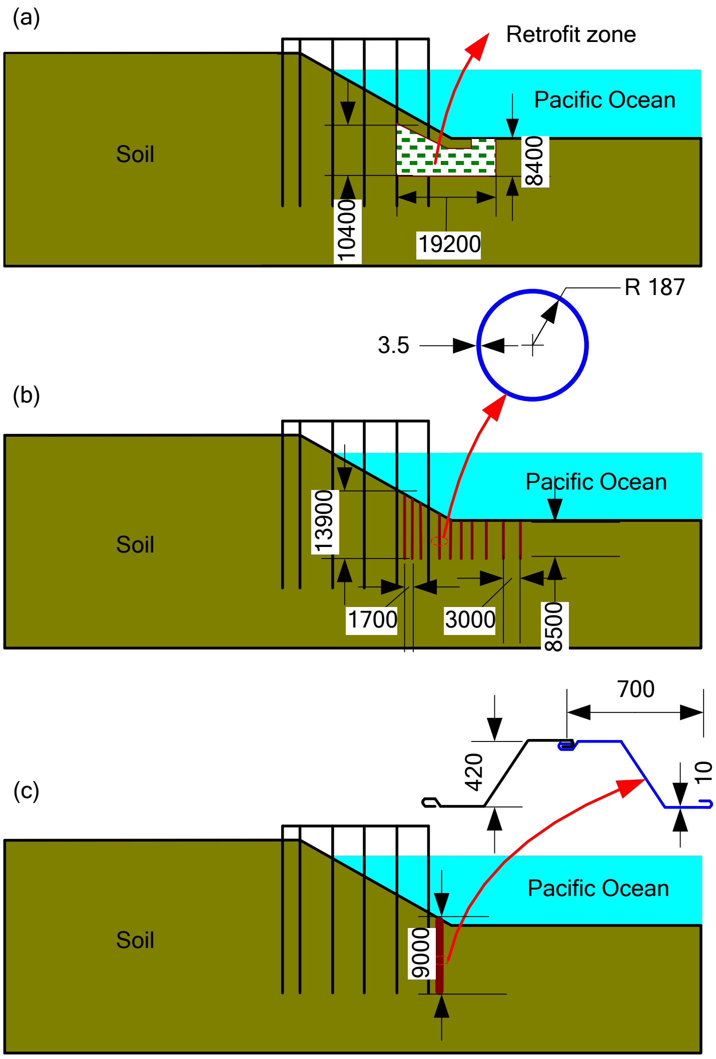


**Figure 3. Schematic of different slope retrofit strategies: (a) Soil-cement mixture; (b) Pin pile; (c) Sheet pile (unit: mm).**

## Finite Element Modeling of As-Built and Retrofitted Pile-Supported Wharf

Since the lateral boundary is far from the pile-supported wharf-ground system and its modeling involves a variety of finite element (FE) types, the target FE simulation domain (shown in Fig. 2a) is selected in an effort to reduce complexity. Specifically, the selected FE simulation domain is 230 m long, and 53.8 m high on the landside, and 33.5 m high on the waterside. The resulting FE models of the as-built and retrofitted wharf structures are shown in Fig. 4. Modeling details are presented in the following sections.

### Modeling of piles and soil domain

The pile cross-section has an octagonal shape and its fiber discretization (Fig. 2e) consists of steel strands, as well as core and cover concrete. As such, the piles are modeled using nonlinear force-based beam-column elements with fiber section. In particular, the core and cover concrete is simulated using *Concrete01* material model (Table 2) in OpenSees. Such model is characterized by a modified Kent-Scott-Park backbone curve with zero stress in tension and degraded linear unloading/reloading stiffness [40-42]. The backbone curve is smoothed by polynomial functions, and the steel is simulated using the uniaxial Giuffre-Menegotto-Pinto model (Table 2) with isotropic strain hardening (i.e., *Steel02* material model in OpenSees). It should be mentioned that initial strain is applied due to the prestressing effect of the steel strands.

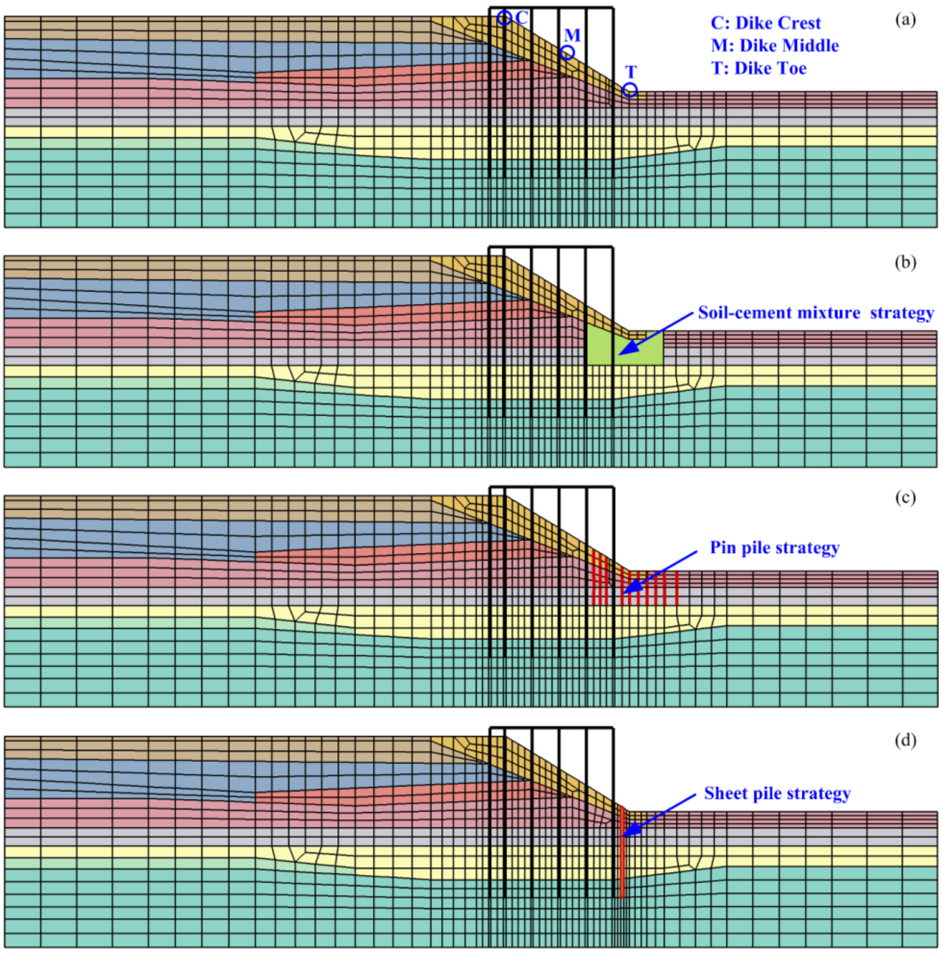


**Figure 4. Finite element mesh for different slope retrofit strategies: (a) As-built; (b) Soil-cement mixture; (c) Pin pile; (d) Sheet pile.**

**Table 2. Properties of concrete and prestressing steel used in fiber section [32].**

| Parameter | Description | Unit | Value |
|---|---|---|---|
| $f_c^{'}$ | Concrete compressive strength | MPa | -74.9 (-49.0) |
| $\varepsilon_c$ | Strain at concrete compressive strength | - | -0.005 (-0.002) |
| $f_{cu}$ | Concrete crushing strength | MPa | -63.0 (0) |
| $\varepsilon_{cu}$ | Strain at concrete crushing strength | - | -0.018 (-0.004) |
| $f_y$ | Steel yield strength, | MPa | 1490 |
| $E$ | Steel elastic modulus | MPa | $2.04\times10^5$ |
| $\sigma_{Init}$ | Prestressing | MPa | 1062 |
| $b$ | Steel strain-hardening ratio | - | 0 |

*Note*: the values outside parentheses represent the properties of confined concrete, while those inside parentheses characterize the properties of unconfined concrete.

The overall soil domain is idealized into 9 sub-layers as well as the dike structure shown in Fig. 1 and Table 1. The saturated soil is modeled using four-node plane-strain bilinear isoparametric elements, to represent the dynamic behavior of this two-phase solid-fluid fully coupled material [43]. Each node has three degrees of freedom (DOFs): two solid displacements and one fluid pressure. For computational convenience, permeability for all soil strata is set to the high value of 1 m/s to mimic a drained condition since liquefaction is not the primary concern due to the relatively high friction angles of the cohesionless strata [36]. The PDMY soil model (i.e., *PressureDependMultiYield* material model in OpenSees) is used to characterize the nonlinear behavior of the saturated sand [44-46]. To be specific, the yield function of the PDMY model follows the classical plasticity convention. It is assumed that the material elasticity is linear and isotropic while the material plasticity is nonlinearity and anisotropy. The yield function forms a conical surface in the stress space with its apex on the hydrostatic axis. A number of similar yield surfaces with a common apex and different size form the hardening zone, and the outermost surface is the envelop of peak shear strength. The flow rule of the PDMY model defines the direction of plastic strain increments using the normality rule. The soil contractive/dilative behavior is governed by a non-associative flow rule. In contrast, the PIMY soil model (i.e., *PressureIndependMultiYield* material model in OpenSees) is used to capture the shear behavior of clay under cyclic loading, which is independent of confinement. The water level is located on the top of loose marine sand (soil layer IIA in Table 1). Above the slope, the water body is simulated by applying hydrostatic pressure on the ground surface on the waterside, imposing effective stresses on the underlying soil layer [47].

**Modeling of soil-pile interaction**

For this large-scale pile-supported wharf, significant soil-pile interaction (SPI) effects are involved and should be taken into account in the FE model. Interface elements developed based on the possible deformation mechanisms of soil-pile interface are effective for simulating SPI [48]. As such, Elgamal et al. [49] employed the rigid link element perpendicular to pile axis with *equalDOF* constraints (i.e., *equalDOF* in OpenSees), which directly connect the soil node and the end node of rigid link element. Such interface modeling can incorporate the effect of pile geometry but fails to characterize the friction and slip mechanism of soil-pile interface during dynamic excitation [49]. Fortunately, this modeling capability can be improved to simulate friction and slip effects of SPI by using an *equalDOF* constraint, zero-length element, and rigid link element to create the connection. In this regard, the zero-length element provides the yield shear force, perpendicular to the axial force to simulate the slip at the soil-pile interface [32]. Herein, the rigid link element is used to characterize the effect of pile diameter, and specifically, the length of the rigid link element is equal to the pile radius. Two types of zero length elements (i.e., *zeroLength* and *zeroLengthSection* in OpenSees) are utilized to model the yield shear force at the soil-pile interface. The *zeroLength* elements aim to axially connect the rigid link element to the corresponding soil nodes. Along the soil-pile interface, the *zeroLengthSection* elements provide the skin-friction yield shear force to simulate the interface slip. Such yield shear force depends on the length and depth of pile elements as well as soil properties (i.e., friction angle and cohesion). The end nodes of rigid link element near soil element connect to the corresponding soil nodes by *equalDOF* constraint.

**Modeling of retrofit strategies**

This section focuses on modeling of retrofit strategies based on their design schematic shown in Fig. 3. Fig. 4 shows the FE mesh of the retrofitted pile-supported wharf with different slope retrofit strategies along with the as-built scenario. For the soil-cement mixture retrofit strategy, the pressure-independent multi-yield surface (PIMY) elastic-plasticity model [50] with a higher cohesion is selected to model the soil-cement mixture. Since deformation compatibility is assumed, no special element is needed to model the interface between soil and mixture. For the pin pile retrofit strategy, the pin piles are simulated by elastic beam column elements. No slip in the soil-pile interface is assumed and thus the nodes of pin piles directly connect to the adjacent soil nodes. For the sheet pile strategy, linear beam elements are used to model the sheet piles. Such modeling technique has been found effective in modeling quay wall systems [51].

**Boundary and loading conditions**

The boundary conditions of the FE models are: (1) lateral boundary is applied by employing a larger size soil column to impose free-field conditions and soil columns on both sides maintain the same properties with the model boundary; (2) nodes at the bottom of the model are fixed in all directions before shaking, and the lateral displacement DOF constraint in the shaking direction is released during shaking; (3) to avoid the spurious wave reflections along the model boundary, the Lysmer-Kuhlemeyer [52] boundary is applied along the model base. In such boundary, three dashpots are defined through the zero length element and the base input motion is applied by the equivalent loading, which is calculated by dashpot coefficient scaled by the area of model base. Following the method of Joyner and Chen [53], the dashpot coefficient is defined as the product of the mass density and shear wave velocity of the underlying medium; and (4) nodal pore pressure is specified on the ground surface on the waterside according to the water height so that the ground surface boundaries on the waterside and landside are pervious.

Both linear and nonlinear procedures are involved for seismic analysis of the wharf-ground system. For the linear procedure, gravity application analysis (self-weight modeling) is performed before seismic excitation. Next, the initial state analysis is enforced to maintain the soil stress states, and soil displacement is initialized to zero through the OpenSees *InitialStateAnalysisWrapper* [54]. The obtained soil stress state serves as the initial condition for the subsequent nonlinear dynamic analysis. To achieve convergence and model the actual loading conditions, a staged analysis scheme is employed for performing the dynamic analysis [55]. Such staged analysis scheme consists of 6 steps: (1) self-gravity of model is performed to obtain the initial stress state for the subsequent analysis; (2) prestressing of pile foundations simulated by nonlinear beam-column element is imposed by applying the initial strain of steel; (3) rigid link element and interface element (i.e., *zeroLength* and *zeroLengthSection* elements in OpenSees) are added to simulate the deck and soil-pile interaction, respectively;

(4) static analysis of SPI system is performed by imposing the self-gravity of deck and pile; (5) properties of soil layers are switched from elastic to plastic, and then the plastic analysis is performed; and (6) soil column with heavy mass are connected on both lateral sides of model through the *equalDOF* to simulate the free field boundary. Eventually, through applying the base motion, the nonlinear time history analysis is conducted to compute seismic response.

## Seismic Response of Retrofitted Pile-Supported Wharf

For seismic performance comparison of the various retrofit strategies, a base excitation with relatively high peak acceleration is employed. Such base excitation aims to produce a noticeable permanent seismic displacement. Fig. 5 shows the target base acceleration time history excitation from Westmorland earthquake (1981) recorded at the 5060 Brawley Airport Station. Following the staged analysis procedure detailed above, seismic responses of the as-built and retrofitted pile-supported wharves can be obtained. The responses under investigation include deck displacement, slope displacement, pile top bending moment and curvature. These four seismic responses are addressed in the subsequent seismic analyses due to the fact that damage and failure of the pile-supported wharves under seismic events is often associated with large slope deformation, excessive deck displacement, and the resulting pile deformation.

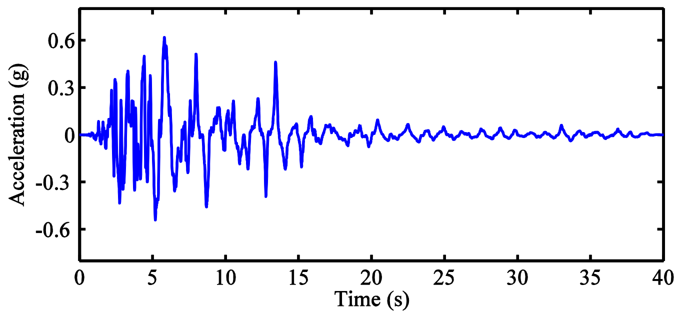


**Figure 5. Representative base excitation.**

Fig. 6 presents a comparison of time history response for various retrofit strategies under the selected ground motion. From Fig. 6(a), it can be observed that deck response of the as-built and retrofitted wharf structures are almost the same before 6 s. As the base excitation continues, the difference gradually increases from 6 to 16 s, and such obvious difference remains stable until the end of shaking. It can be seen that deck displacement becomes smaller after seismic retrofit, as anticipated. Among these three retrofit strategies, the soil-cement mixture retrofit results in the minimum deck displacement, the sheet pile comes second, followed by the pin pile approach. Fig. 6(b) shows the influence of the three retrofit strategies on the slope displacements at representative locations (i.e., crest, middle, and toe of slope, shown in Fig. 4a). Compared to the as-built case, these three retrofit strategies effectively restrain the development of slope deformation. The pin pile retrofit technique presents the best performance for slope displacement mitigation, followed by soil-cement mixture, and finally sheet pile retrofit. Fig. 6(c) exhibits the effect of the retrofit strategies on the pile top bending moment. For the sake of brevity, the seismic response of Piles A and F are presented. Pile A has maximum free length while Pile F has minimum free length, and in addition, the Pile A is closest to the retrofit zone while the Pile F is farthest. The retrofit strategies have minimal effect on bending moment at the top of Pile F but affect the bending moment at the top of Pile A. It can be seen that among these retrofit strategies, the soil-cement mixture most significantly mitigates the bending moment of Pile A near the top. The influence of different slope retrofit strategies on the curvature at pile top is displayed in Fig. 6(d). In contrast to the pile top bending moment, the retrofit strategies have more distinct influence on the pile top curvature. It is interesting to note that after seismic retrofit, curvature at the top of Pile F becomes smaller but curvature at the top of Pile A becomes larger. The observed response of Piles A and F indicate that the retrofit strategies mainly influence the seismic response of soil and pile in the vicinity of the retrofit zone.

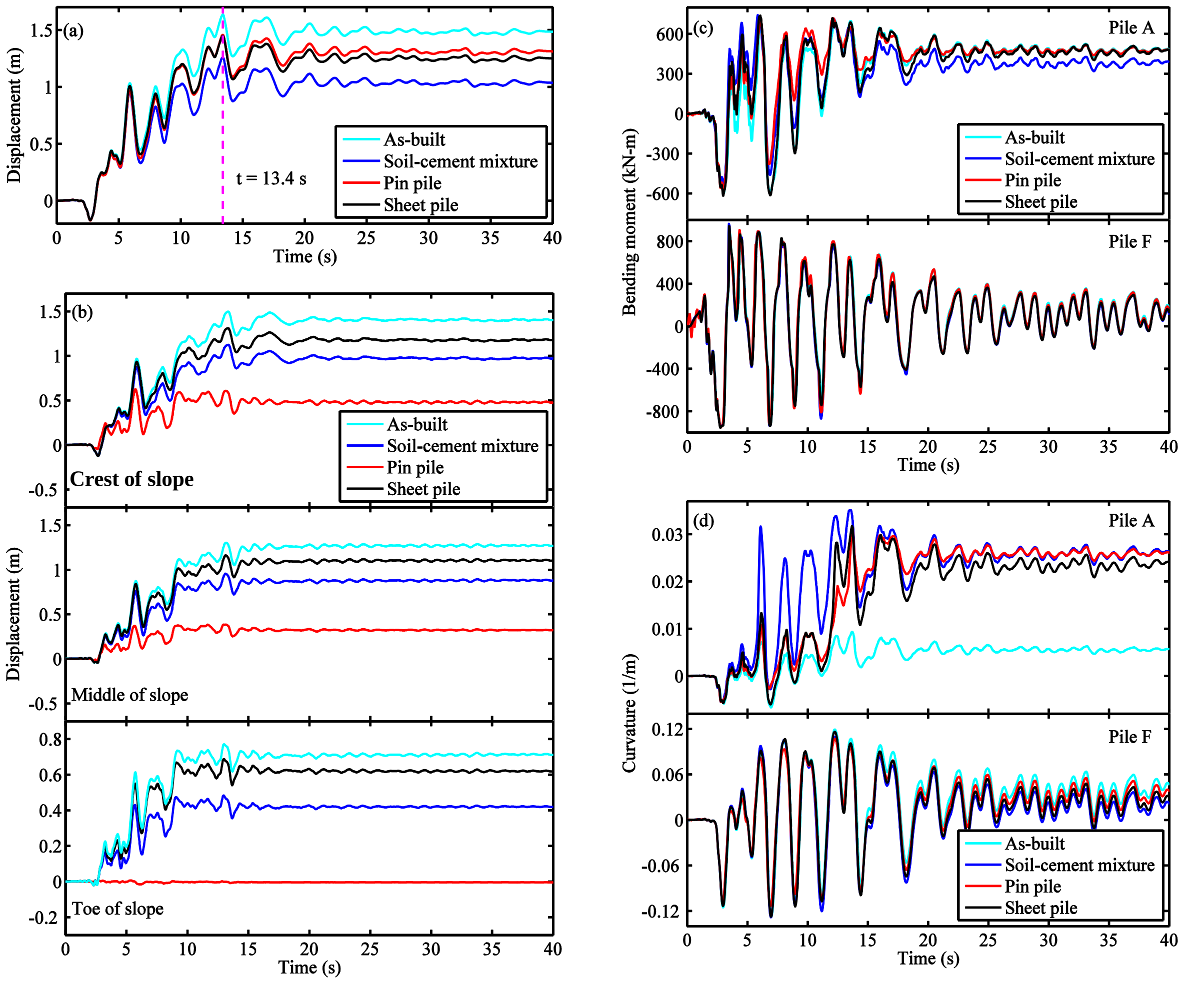


**Figure 6. Comparison of time history response for different slope retrofit strategies: (a) Deck displacement; (b) Slope displacement; (c) Bending moment on Piles A and F top; (d) Curvature on Piles A and F top.**

Fig. 7 displays lateral deformation of the wharf-ground system with and without the different slope retrofit strategies at the time instant of the maximum deck displacement (i.e., 13.4 s in Fig. 6a). Generally, these three retrofit strategies effectively restrict the lateral slope displacement, and the maximum slope displacement occurs on the crest of slope. The deformation zone of soil-cement mixture retrofit strategy is similar to that of the as-built case, except the slope toe. The pin pile retrofit strategy evidently shrinks the deformation area, and deformation of the slope toe and the deeper soil domain is largely diminished. The sheet pile retrofit strategy produces a similar deformation area to the as-built case but in general, the displacement response is relatively small.

To better understand the impact of the retrofit strategies on the wharf structure, lateral deformation of the wharf structure before and after seismic retrofit is investigated. Fig. 8 presents the comparison of lateral deformation profiles of the wharf structure with and without retrofit at the time instant of the maximum deck displacement (i.e., 13.4 s in Fig. 6a). It is clear that the three retrofit strategies play an essential role in decreasing lateral deformation of the wharf structure, especially for the soil-cement mixture case. Compared to the soil-cement mixture and sheet pile retrofit techniques, the pin pile retrofit efficiently diminishes the pile deformation at deeper depths as shown in Fig. 8.

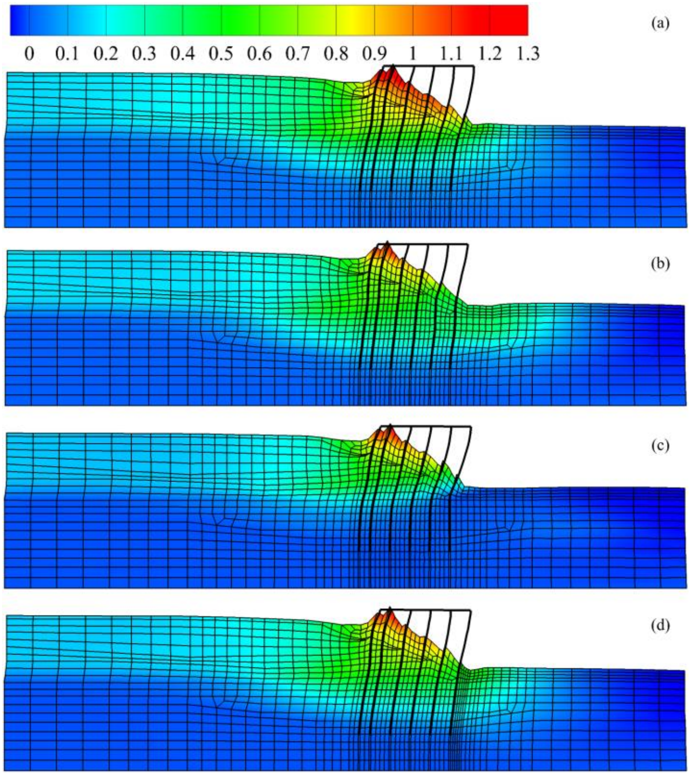


**Figure 7. Lateral deformation of wharf-ground system at the time interval of maximum deck displacement for different slope retrofit strategies (t = 13.4 s shown in Fig. 6a): (a) As-built; (b) Soil-cement mixture; (c) Pin pile; (d) Sheet pile; (Unit: m, scaling factor of 5 for visualization).**

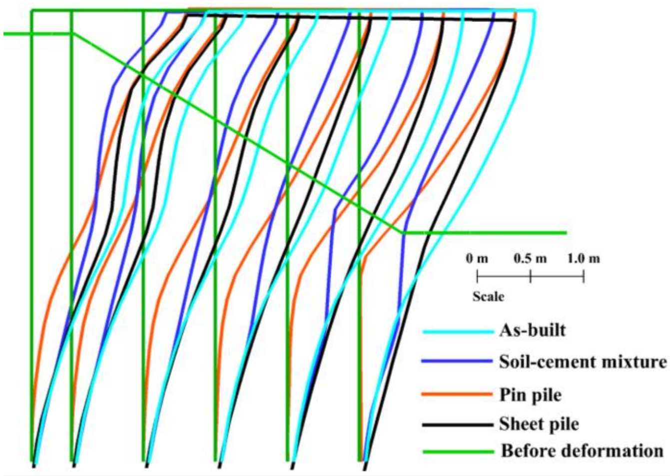


**Figure 8. Lateral deformation of wharf structure at the time interval of maximum deck displacement (t = 13.4 s shown in Fig. 6a, scaling factor of 10 for visualization).**

In line with the above observations, it can be concluded that the effects of the different slope retrofit strategies on seismic response of this wharf-ground system are distinct. That is to say, the retrofit strategy exhibits that less effectiveness in mitigating a certain seismic response can be more efficient in reducing other seismic responses. For example, the pin pile retrofit demonstrated greater capability in lowering displacements of the soil stratum, but that was not the case for the deck displacement. For the deck displacement, the soil-cement mixture retrofit was the most effective. As a consequence, the appropriate retrofit strategy should be determined according to the specific improvement objective, in terms of reducing seismic response of the soil strata versus the wharf structure.

## Seismic Fragility of Retrofitted Pile-Supported Wharf

### Fragility analysis methodology

Fragility curves provide an effective and practical means to measure the capability of a structure to withstand a specified event [56-58]. Specifically, seismic fragility defines the conditional probability of the seismic demand (*D*) placed upon the structure equal to or greater than its capacity (*C*) for a given ground motion intensity measure (*IM*). The conditional probability can be expressed in the following form [56]

$$\text{Fragility}=P\left(D \geq C \mid IM\right) \tag{1}$$

Evaluation of seismic fragility starts with construction of a probabilistic seismic demand model (PSDM) that is used to correlate the engineering demand parameters (EDPs) with the *IM* and represent a probability distribution for the demand. Often, it is assumed that the EDP follows a two-parameter lognormal probability distribution whose median is characterized by a power-law model [59], such that

$$S_D = a\, IM^{b} \tag{2}$$

where $S_D$ is the median estimate of the seismic demand, and $a$ and $b$ are the power-law model parameters. The Eq. (2) can be equivalently expressed in logarithmic space, taking linear form

$$\ln\left(S_D\right) = \ln(a) + b\ln\left(IM\right) \tag{3}$$

which facilitates the estimation of the power-law model coefficients $a$ and $b$ using a linear regression estimator. As mentioned above, the PSDM is modeled as a lognormal distribution, so it can be formulated as [60]

$$P\left(D \geq d \mid IM\right) = 1 - \Phi\left[\frac{\ln\left(d\right) - \ln\left(S_D\right)}{\beta_{D|IM}}\right] \tag{4}$$

$$\beta_{D|IM} = \sqrt{\frac{\sum_{i=1}^{n}\left[\ln\left(d_i\right) - \ln\left(S_D\right)\right]^2}{n-2}} \tag{5}$$

where $\Phi(\bullet)$ represents the cumulative standard normal distribution function; $d_i$ is the $i$th realization of the seismic demand; and $n$ is the number of nonlinear time history analyses.

Like the PSDM, the capacity models are also characterized by a two-parameter lognormal distribution. Having the demand and capacity models both defined through the lognormal distribution, the component fragility conditioned on the selected *IM* can be calculated from

$$P(D \geq C \mid IM) = \Phi\left[\frac{\ln(S_D) - \ln(S_C)}{\sqrt{\beta_{D|IM}^2 + \beta_C^2}}\right] \tag{6}$$

where $S_D$ is the median estimate of the demand as a function of $IM$; $S_C$ is the median estimate of the capacity; $\beta_{D|IM}$ is the dispersion or logarithmic standard deviation of the seismic demand conditioned on $IM$; and $\beta_C$ is the dispersion of the capacity.

Compared to the component-level fragility, the system-level fragility allows for global assessment of the seismic vulnerability of the whole wharf system. Seismic vulnerability for a structure system can be readily achieved by combining the effects of various structural components through the use of joint PSDM (JPSDM) [60]. The JPSDM is to formulate the joint probability distribution of the seismic demands by considering the correlation between the transformed demands of various structural components. Specifically, in the log-transformed state, the transformed seismic demands follow a multivariate normal distribution [60]. The mean vector is computed by Eq. (3), and the covariance matrix is assembled through estimation of the correlation coefficients between the transformed demands placed on the various components [52]. The covariance matrix associated with the JPSDM is calculated using the results of nonlinear time history analyses (NLTHA) corresponding to a suite of selected ground motions. Since the NLTHA are already performed for the component-level fragility calculation, no more NLTHA are needed for construction of JPSDM. Bear in mind that the log-transformed capacities also follow normal distribution.

After the joint probability models of seismic demands and capacities are obtained, the system-level fragility can be estimated via a Monte Carlo simulation (MCS). To be specific, Latin hypercube sampling (LHS) is employed to draw samples based on the obtained seismic demand and capacity probability models. A large number of samples are generated through the LHS algorithm using the probabilistic characterization of the demand estimated from the NLTHA data and capacity postulated. Using the generated samples, the MCS estimate of system failure probability at given $IM$ is defined by [34]

$$P_{F_S} = \frac{1}{N}\sum_{i=1}^{N} I(\mathbf{x}_{C,i}, \mathbf{x}_{D,i}) \tag{7}$$

where $I(\bullet)$ denotes the failure indicator function. This study adopts an assumption of a serial system that no failure is claimed only when the capacity of all the components is higher than the corresponding demand. The failure indicator function can be calculated from [34]

$$I(\mathbf{x}_{C,i}, \mathbf{x}_{D,i}) = \begin{cases} 0 & \text{if} \quad x_{C,i1} > x_{D,i1} \text{ and } x_{C,i2} > x_{D,i2} \text{ and } \cdots \text{ and } x_{C,im} > x_{D,im} \\ 1 & \text{Otherwise} \end{cases} \tag{8}$$

in which $\mathbf{x}_{C,i}$ and $\mathbf{x}_{D,i}$ are the $i$th samples associated with the seismic demand and capacity, respectively; and $m$ is the number of structural components under consideration.

## Fragility analysis results

A suite of 80 ground motions are selected for seismic fragility analysis [61]. These ground motions are extracted from the Pacific Earthquake Engineering Research Center Strong Motion Database [62]. These selected ground motions have an even selection of recorded time histories from four bins that include combinations of low and high moment magnitudes, as well as large and small fault distances. The ground motion selection criteria are: (1)

the California ground motions recorded on site class D are under consideration since the selected wharf is located in California and its site type belongs to class D and (2) the chosen ground motions have various moment magnitudes as well as fault distances to be more representative.

Because the deck displacement, bending moment and pile top curvature are the important indicators of wharf structure seismic performance, these response quantities are used as demands for seismic fragility assessment [34]. Based on the above-mentioned FE modeling procedures, nonlinear time history analysis is carried out for each of the selected 80 ground motions to obtain the seismic responses of interest. A data set of 80 *IM-D* pairs is used for subsequent seismic fragility analysis.

Before performing fragility analysis, the quantitative seismic demand bounds for different damage states need to be defined. In this study, three damage states (i.e., slight, moderate, and extensive damage states) are considered. The slight damage state corresponds to the cover concrete strain on pile at crushing strength (i.e., 0.004 in Table 2); the extensive damage state corresponds to the core concrete strain on pile at crushing strength (i.e., 0.018 in Table 2); and the moderate damage state is assumed to be the core concrete strain of 0.01, which is close to the average of the slight and extensive damage levels.

Fragility curves at the component level can be derived based on Eq. (6). The results of the component fragility curves of this wharf structure before and after seismic retrofit are shown in Figs. 9-13. For various retrofit strategies as well as the as-built case, the fragility curves associated with the deck displacement-specific seismic demand are compared in Fig. 9, which offers a clear picture of how damage exceedance probability (fragility) for each damage state corresponds to the different peak ground velocity (PGV) levels. Using the retrofit techniques, the seismic fragility of the wharf deck turns out to be smaller, and the seismic fragility reduction becomes more significant from small to large damage states. As seen from Fig. 9, the soil-cement mixture retrofit strategy provides the best performance for lowering the seismic fragility of the wharf deck, followed by the pin pile, and then the sheet pile. Their performance differences can be mainly illustrated by their displacements, as shown in Fig. 6 (a), in which it can be seen that the soil-cement mixture retrofit measure corresponds to the minimum deck displacement, followed by that of the sheet pile and the pin pile.

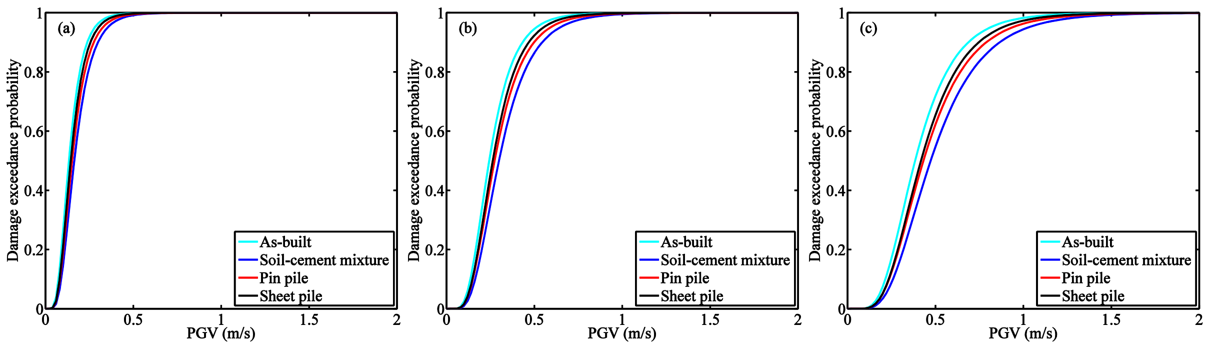


**Figure 9. Damage exceedance probability of deck displacement: (a) Slight damage state; (b) Moderate damage state; (c) Extensive damage state.**

Figs. 10 and 11 present the fragility curves of bending moments at the top of Piles A and F, respectively. Like the deck displacement, overall, the damage exceedance probabilities of bending moments for various retrofit strategies are smaller than those for the as-built case, and the damage exceedance probabilities gradually decrease from the slight to extensive damage states (Figs. 10 and 11). It can be also observed that the pile bending moment-specific seismic fragility is significantly smaller than the deck displacement-specific seismic fragility for both unretrofitted and retrofitted scenarios. Fig. 10 indicates that not all retrofit measures are effective in reducing the bending moment-specific seismic fragility of Pile A. Particularly, the seismic fragility curves for sheet pile retrofit strategy closely agree with those for the as-built case, and again, the soil-cement mixture retrofit strategy performs best.

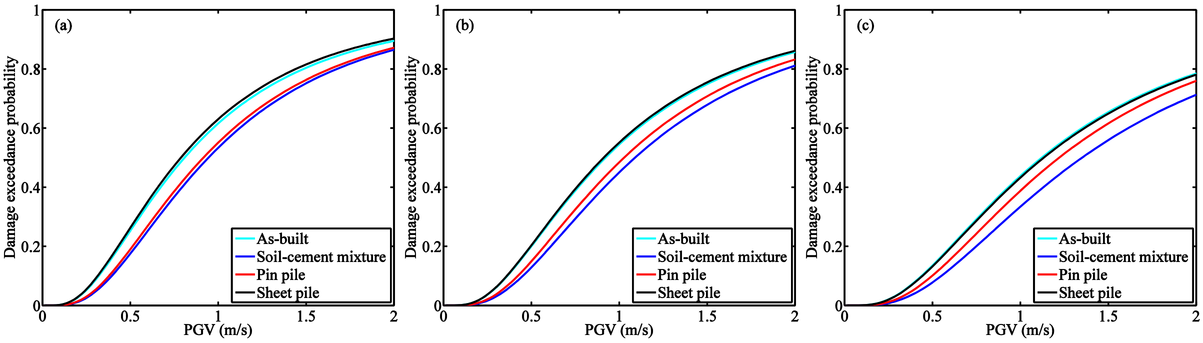


**Figure 10. Damage exceedance probability of bending moment on Pile A top: (a) Slight damage state; (b) Moderate damage state; (c) Extensive damage state.**

Fig. 11 reveals that the effects of various retrofit strategies on the bending moment-specific seismic fragility of Pile F top are quite obvious. Compared to the Pile A, the differences of fragility curves associated with the various retrofit strategies are more noticeable for Pile F. As seen from Fig. 11, the performance rank of the retrofit measures in descending order is: soil-cement mixture, pin pile, and sheet pile. Generally, the retrofit strategies are effective in reducing the bending moment-specific seismic fragility.

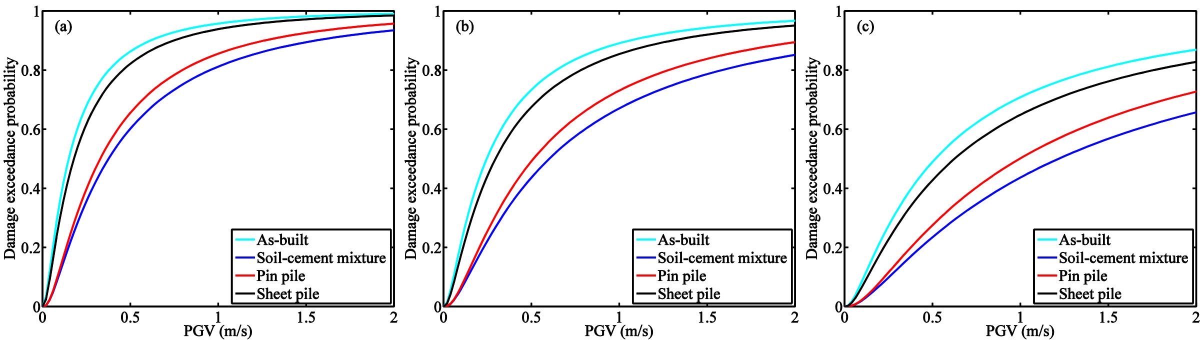


**Figure 11. Damage exceedance probability of bending moment on Pile F top: (a) Slight damage state; (b) Moderate damage state; (c) Extensive damage state.**

Figs. 12 and 13 depict the fragility curves of curvature at the top of Piles A and F, respectively. Overall, the various retrofit strategies increase the curvature-specific seismic vulnerability of Pile A, which means that the retrofit schemes have a negative effect on seismic risk mitigation of Pile A. On the other hand, these retrofit measures positively affect the curvature-specific seismic fragility of Pile F slightly. Therefore, one can conclude that the influence of the retrofit strategies on the seismic fragilities of different piles is not identical. Combined with Figs. 10 and 11, it can be seen that the impacts of the retrofit strategies on seismic damage mitigation can be different even for the same pile when using different seismic demands (i.e., bending moment or curvature) in seismic analysis. This may be explained by the evidence revealed by Fig. 6 that the impact of the same retrofit technique on different types of seismic responses can be inconsistent. The results of component fragility analysis demonstrate that one retrofit strategy cannot decrease the seismic vulnerabilities associated with different seismic demands of all structural components, which demonstrates that identification of the effective retrofit strategy should be performed in accordance with the particular improvement objective.

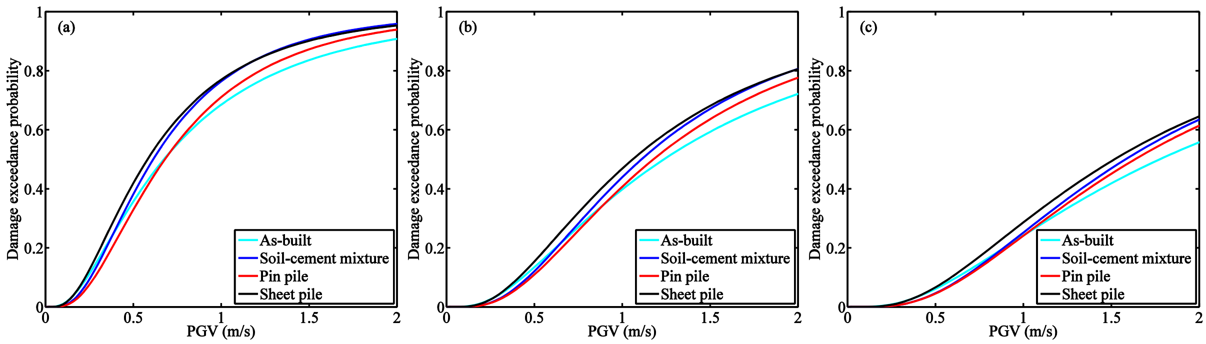


**Figure 12. Damage exceedance probability of curvature on Pile A top: (a) Slight damage state; (b) Moderate damage state; (c) Extensive damage state.**

The component fragility analysis of the pile-supported wharf before and after seismic retrofit shows a clear picture of effectiveness in reducing the seismic damage of the wharf structure at a component level. To assess the effect of various retrofit strategies on the overall fragility of the wharf structure, the system fragility analysis needs to be addressed. The system fragility analysis allows modelers to have a macroscopic view of the seismic fragility of the whole wharf system. Based on the JPSDM principle described above, the results of system seismic fragility can be obtained (Fig. 14). It can be seen that the wharf structure becomes less susceptible to seismic damage after retrofit. More specifically, for all slight, moderate, and extensive damage states, performance of the soil-cement mixture retrofit strategy in terms of the system seismic fragility mitigation is best, followed by the pin pile. Effect of the sheet pile retrofit is also positive but quite small. As such, the system fragility analysis enables evaluation of seismic performance of the various retrofit strategies in a combined manner. It should be noted that unlike the component fragilities and seismic responses, the system fragilities exhibit slight difference for these slope strengthening strategies. This is because these strengthening strategies focus on the slope (local) improvement whereas the system fragility is a global term.

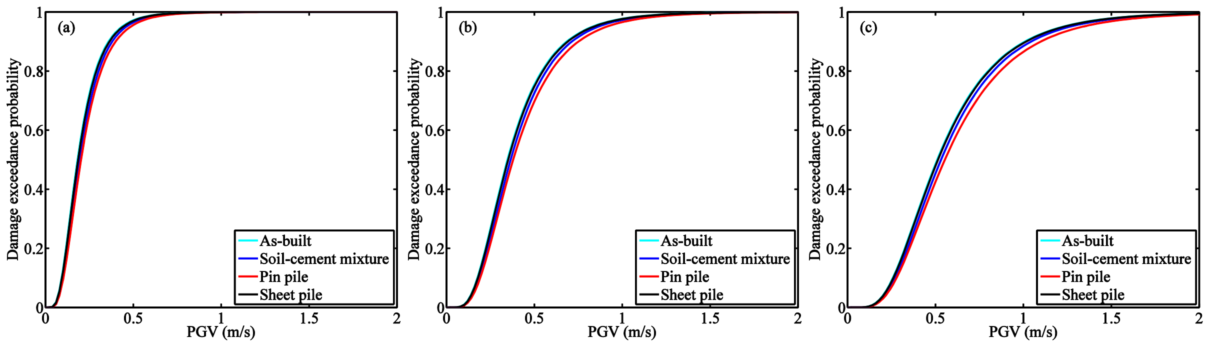


**Figure 13. Damage exceedance probability of curvature on Pile F top: (a) Slight damage state; (b) Moderate damage state; (c) Extensive damage state.**

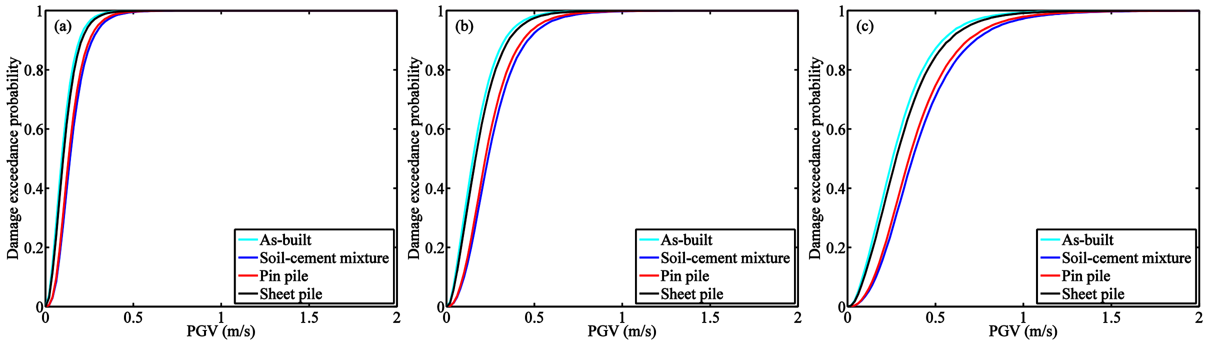


**Figure 14. Damage exceedance probability of the wharf system: (a) Slight damage state; (b) Moderate damage state; (c) Extensive damage state.**

## Concluding Remarks

This paper focuses on seismic performance assessment of a large-scale pile-supported wharf retrofitted with different slope strengthening strategies. Since there exists a weak clay stratum with low shear modulus and cohesion below the dike section, the safety reserve of the dike section against excessive deformation may not be adequate under potential seismic events. Three seismic retrofit measures are studied for slope improvement of the existing wharf dike, namely, improving the ground by a soil-cement mixture, driving pin piles near the dike toe, and creating an underwater bulkhead system using sheet piles. Seismic performance of these retrofit strategies on the wharf structure system is evaluated systematically from two perspectives. First, the seismic responses (slope deformation, wharf deck displacement, and pile top bending moment and curvature) of the pile-supported wharf with and without retrofit measures under a representative ground motion are fully investigated. Second, within a probabilistic framework, the effectiveness of various retrofit strategies in seismic damage mitigation of the pile-supported wharf is assessed using a versatile fragility analysis scheme. Seismic fragilities of the wharf structure before and after seismic retrofit are thoroughly evaluated in both component- and system-level manners. The conclusions drawn from this study include:

- Generally, under the selected representative ground motion, the retrofit strategies played a significant role in mitigating the seismic response of the pile-supported wharf. Particularly, the soil-cement mixture retrofit performed best, being most effective in reducing lateral deformation of the wharf structure.
- It should be noted that a given retrofit measures can have an unexpected negative impact on certain seismic responses of particular structural component. For example, curvature at the top of Pile A becomes larger after retrofit. Hence, the appropriate retrofit strategy should be determined according to the specific improvement objective, such as seismic response mitigation of the soil stratums or the wharf structure.
- After retrofit, the wharf deck was less susceptible to seismic damage, and among these retrofit strategies, the soil-cement mixture retrofit provided the best performance for lowering seismic fragility of the wharf deck. Overall, the three retrofit strategies are effective for alleviating the seismic vulnerability of the piles, despite increasing the curvature-specific seismic vulnerability of Pile A. In addition, the soil-cement mixture retrofit does not always perform best for decreasing the seismic fragilities of the piles. This reveals that effects of various retrofit strategies on seismic risk mitigation of different structural components can be different and sometimes, certain retrofit measure may have a localized negative impact.
- From the perspective of system-level seismic fragility, all retrofit strategies resulted in positive influences in terms of lowering the global seismic fragility of the overall wharf structure. Specifically, the soil-cement mixture retrofit in the system seismic fragility mitigation results in the lowest damage exceedance

probability, followed by the pin pile, and then by the sheet pile.


## Acknowledgements

This research was financially supported by the National Key Research and Development Program of China (2016YFE0205100), and the National Natural Science Foundation of China (51578494, 51808307 and 51878235).


## References


[1] EQE. (1989) The October 17, 1989 Loma Prieta Earthquake. Prepared by EQE Engineering Inc. Report.

[2] Chung RM. (1996) The January 17, 1995 Hyōgo-ken-Nanbu (Kobe) Earthquake: Performance of structures, lifelines, and fire protection systems. US Department of Commerce, Technology Administration, National Institute of Standards and Technology.

[3] Green RA, Olson SM, Cox BR, Rix GJ, Rathje E, Bachhuber J, French J, Lasley S, Martin N. (2011) Geotechnical aspects of failures at Port-au-Prince Seaport during the 12 January 2010 Haiti Earthquake. Earthquake Spectra; 27(S1):43-65.

[4] Applied Technology Council and Multidisciplinary Center for Earthquake Engineering Research. (2003) Recommended LFRD guidelines for the seismic design of highway bridges. MCEER/ATC-49, Redwood City, CA.

[5] Erdogan H, Doran B, Seckin A, Akbas B, Celikoglu Y, Bostan T. (2017) Seismic performance and retrofit evaluation of an existing pile-wharf structure. Journal of Performance of Constructed Facilities; 31(6):04017110.

[6] Kim SH, Shinozuka M. (2004) Development of fragility curves of bridges retrofitted by column jacketing. Probabilistic Engineering Mechanics; 19(1-2):105-112.

[7] Casciati F, Cimellaro GP, Domaneschi M. (2008) Seismic reliability of a cable-stayed bridge retrofitted with hysteretic devices. Computers & Structures; 86(17-18):1769-1781.

[8] Padgett JE, DesRoches R. (2008) Methodology for the development of analytical fragility curves for retrofitted bridges. Earthquake Engineering & Structural Dynamics; 37(8):1157-1174.

[9] Padgett JE, DesRoches R. (2009) Retrofitted bridge fragility analysis for typical classes of multispan bridges. Earthquake Spectra; 25(1):117-141.

[10] Zhang J, Huo Y. (2009) Evaluating effectiveness and optimum design of isolation devices for highway bridges using the fragility function method. Engineering Structures; 31(8):1648-1660.

[11] Xie Y, Zhang J. (2018) Design and optimization of seismic isolation and damping devices for highway bridges based on probabilistic repair cost ratio. Journal of Structural Engineering; 144(8):04018125.

[12] Billah AHMM, Alam MS, Bhuiyan MAR. (2013) Fragility analysis of retrofitted multicolumn bridge bent subjected to near-fault and far-field ground motion. Journal of Bridge Engineering; 18(10):992-1004.

[13] Billah AHMM, Alam MS. (2014) Seismic performance evaluation of multi-column bridge bents retrofitted with different alternatives using incremental dynamic analysis. Engineering Structures; 62-63:105-117.

[14] Zakeri B, Padgett JE, Ghodrati Amiri G. (2015) Fragility assessment for seismically retrofitted skewed reinforced concrete box girder bridges. Journal of Performance of Constructed Facilities; 29(2):04014043.

[15] DesRoches R, Delemont M. (2002) Seismic retrofit of simply supported bridges using shape memory alloys. Engineering Structures; 24(3):325-332.

[16] Zheng Y, Dong Y, Li Y. (2018) Resilience and life-cycle performance of smart bridges with shape memory

alloy (SMA)-cable-based bearings. Construction and Building Materials; 158:389-400.
[17] Abbasi M, Moustafa MA. (2019) Probabilistic seismic assessment of as-built and retrofitted old and newly designed skewed multi-frame bridges. Soil Dynamics and Earthquake Engineering; 119:170-186.
[18] Di Sarno L, Manfredi G. (2010) Seismic retrofitting with buckling restrained braces: Application to an existing non-ductile RC framed building. Soil Dynamics and Earthquake Engineering; 30(11):1279-1297.
[19] Sorace S, Terenzi G. (2017) Existing prefab R/C industrial buildings: seismic assessment and supplemental damping-based retrofit. Soil Dynamics and Earthquake Engineering; 94:193-203.
[20] Mazza F, Mazza M, Vulcano A. (2018) Base-isolation systems for the seismic retrofitting of r.c. framed buildings with soft-storey subjected to near-fault earthquakes. Soil Dynamics and Earthquake Engineering; 109:209-221.
[21] Roeder CW, Graff R, Soderstrom J, Yoo JH. (2005) Seismic performance of pile-wharf connections. Journal of Structural Engineering; 131(3):428-437.
[22] Donahue MJ, Dickenson SE, Miller TH, Yim SC. (2005) Implications of the observed seismic performance of a pile-supported wharf for numerical modeling. Earthquake Spectra; 21(3):617-634.
[23] Blandon CA, Bell JK, Restrepo JI, Weismair M, Jaradat O, Yin P. (2010) Assessment of seismic performance of two pile-deck wharf connections. Journal of Performance of Constructed Facilities; 25(2):98-104.
[24] Chiou JS, Chiang CH, Yang HH, Hsu SY. (2011) Developing fragility curves for a pile-supported wharf. Soil Dynamics and Earthquake Engineering; 31(5-6):830-840.
[25] Yang CSW, DesRoches R, Rix GJ. (2012) Numerical fragility analysis of vertical-pile-supported wharves in the western United States. Journal of Earthquake Engineering; 16(4):579-594.
[26] Shafieezadeh A, DesRoches R, Rix GJ, Werner SD. (2012) Seismic performance of pile-supported wharf structures considering soil-structure interaction in liquefied soil. Earthquake Spectra; 28(2):729-757.
[27] Shafieezadeh A, DesRoches R, Rix GJ, Werner SD. (2012) Three-dimensional wharf response to far-field and impulsive near-field ground motions in liquefiable soils. Journal of Structural Engineering; 139(8):1395-1407.
[28] Doran B, Shen J, Akbas B. (2013) Seismic evaluation of existing wharf structures subjected to earthquake excitation: Case study. Earthquake Spectra; 31(2):1177-1194.
[29] Chiaramonte MM, Arduino P, Lehman DE, Roeder CW. (2013) Seismic analyses of conventional and improved marginal wharves. Earthquake Engineering & Structural Dynamics; 42(10):1435-1450.
[30] Heidary-Torkamani H, Bargi K, Amirabadi R. (2014) Seismic vulnerability assessment of pile-supported wharves using fragility curves. Structure and Infrastructure Engineering; 10(11):1417-1431.
[31] Heidary-Torkamani H, Bargi K, Amirabadi R, McCllough NJ. (2014) Fragility estimation and sensitivity analysis of an idealized pile-supported wharf with batter piles. Soil Dynamics and Earthquake Engineering; 61-62:92-106.
[32] Su L, Lu J, Elgamal A, Arulmoli AK. (2017) Seismic performance of a pile-supported wharf: Three-dimensional finite element simulation. Soil Dynamics and Earthquake Engineering; 95:167-179.
[33] Su L, Wan HP, Dong Y, Frangopol D M, Ling XZ. (2018) Efficient uncertainty quantification of wharf structures under seismic scenarios using Gaussian process surrogate model. Journal of Earthquake Engineering; 1-22.
[34] Su L, Wan HP, Bi K, Li Y, Lu J, Ling XZ, Elgamal A, Arulmoli AK. (2019) Seismic fragility analysis of pile-supported wharves with the influence of soil permeability. Soil Dynamics and Earthquake Engineering; 186:270-281.
[35] Banayan-Kermani A, Bargi K, Heidary-Torkamani H. (2016) Seismic performance assessment of

pile-supported wharves retrofitted by carbon fibre-reinforced polymer composite considering ageing effect. Advances in Structural Engineering; 19(4):581-598.

[36] Earth Mechanics, Inc. (EMI). (2001) Final geotechnical and seismic analyses and design report berth 100 container wharf, west basin Port of Los Angeles, San Pedro, California. Prepared by EMI, submitted to Port of Los Angeles, California.

[37] da Fonseca AV, Cruz RC, Consoli NC. (2009) Strength properties of sandy soil-cement admixtures. Geotechnical and Geological Engineering; 27(6):681-686.

[38] Fan J, Wang D, Qian D. (2018) Soil-cement mixture properties and design considerations for reinforced excavation. Journal of Rock Mechanics and Geotechnical Engineering; 10:791-797.

[39] Richards TD, Rothbauer MJ. (2004) Lateral loads on pin piles (micropiles). In GeoSupport 2004: Drilled Shafts, Micropiling, Deep Mixing, Remedial Methods, and Specialty Foundation Systems; 158-174.

[40] Kent DC, Park R. (1971) Flexural members with confined concrete. Journal of the Structural Division; 97(7):1969-1990

[41] Scott B, Park R, Priestley M. (1982) Stress-strain behavior of concrete confined by overlapping hoops at low and high strain rates. ACI Journal Proceedings; 79(1):13-27.

[42] Mander JB, Priestley MJ, Park R (1988) Theoretical stress-strain model for confined concrete. Journal of Structural Engineering; 114(8):1804-1826.

[43] Yang Z, Elgamal A. (2002) Influence of permeability on liquefaction-induced shear deformation. Journal of Engineering Mechanics; 128(7):720-729.

[44] Elgamal A, Yang Z, Parra E, Ragheb A. (2003) Modeling of cyclic mobility in saturated cohesionless soils. International Journal of Plasticity; 19(6):883-905.

[45] Yang Z, Elgamal A, Parra E. (2003) Computational model for cyclic mobility and associated shear deformation. Journal of Geotechnical and Geoenvironmental Engineering; 129(12):1119-1127.

[46] Khosravifar A, Elgamal A, Lu J, Li J. (2018) A 3D model for earthquake-induced liquefaction triggering and post-liquefaction response. Soil Dynamics and Earthquake Engineering; 110:43-52.

[47] Vytiniotis A. (2001) Contributions to the analysis and mitigation of liquefaction in loose sand slopes. PhD Thesis. Massachusetts Institute of Technology.

[48] Desai C, Nagaraj B. (1988) Modeling for cyclic normal and shear behavior of interfaces. Journal of Engineering Mechanics; 114(7):1198-1217.

[49] Elgamal A, Yan L, Yang Z, Conte JP. (2008) Three-dimensional seismic response of Humboldt Bay bridge-foundation-ground system. Journal of Structural Engineering; 134(7):1165-1176.

[50] Yang Z, Lu J, Elgamal A. (2008) OpenSees soil models and solid-fluid fully coupled elements. User's Manual. Ver, 1.0.

[51] Su L, Wan HP, Li Y, Ling XZ. (2018) Soil-pile-quay wall system with liquefaction-induced lateral spreading: experimental investigation, numerical simulation, and global sensitivity analysis. Journal of Geotechnical and Geoenvironmental Engineering; 144(11):04018087.

[52] Lysmer J, Kuhlemeyer AM. (1969) Finite dynamic model for infinite media. Journal of the Engineering Mechanics Division; 95:859-877.

[53] Joyner WB, Chen ATF. (1975) Calculation of nonlinear ground response in earthquakes. Bulletin of the Seismological Society of America; 65(5):1315-1336.

[54] McGann C, Arduino P, Mackenzie-Helnwein P. (2011) InitialStateAnalysisWrapper. http://opensees.berkeley.edu/wiki/index.php/InitialStateAnalysisWrapper.

[55] Chiaramonte MM. (2011) An analysis of conventional and improved marginal wharves. PhD Thesis, University of Washington.

[56] Tekie PB, Ellingwood BR. (2003) Seismic fragility assessment of concrete gravity dams. Earthquake Engineering & Structural Dynamics; 32(14):2221-2240.

[57] Padgett JE, DesRoches R. (2007) Sensitivity of seismic response and fragility to parameter uncertainty. Journal of Structural Engineering; 133(12):1710-1718.

[58] Dong Y, Frangopol DM, Saydam D. (2013) Time-variant sustainability assessment of seismically vulnerable bridges subjected to multiple hazards. Earthquake Engineering & Structural Dynamics; 42(10):1451-1467.

[59] Cornell CA, Jalayer F, Hamburger RO, Foutch DA. (2002) Probabilistic basis for 2000 SAC federal emergency management agency steel moment frame guidelines. Journal of Structural Engineering; 128(4):526-533.

[60] Nielson BG, DesRoches R. (2007) Seismic fragility methodology for highway bridges using a component level approach. Earthquake Engineering & Structural Dynamics; 36(6):823-839.

[61] Ramanathan K, Jeon JS, Zakeri B, DesRoches R, Padgett JE. (2015) Seismic response prediction and modeling considerations for curved and skewed concrete box-girder bridges. Earthquakes and Structures; 9(6):1153-1179.

[62] Medina RA, Krawinkler H. (2004) Seismic demands for nondeteriorating frame structures and their dependence on ground motions. PEER Report 2003/15.

# Conflict of Interest

- All authors have participated in (a) conception and design, or analysis and interpretation of the data; (b) drafting the article or revising it critically for important intellectual content; and (c) approval of the final version.

- This manuscript has not been submitted to, nor is under review at, another journal or other publishing venue.

- The authors have no affiliation with any organization with a direct or indirect financial interest in the subject matter discussed in the manuscript


| Author's name | Affiliation |
|---|---|
| Lei Su | Qingdao University of Technology, China |
| Hua-Ping Wan | Zhejiang University, China |
| Yaozhi Luo | Zhejiang University, China |
| You Dong | The Hong Kong Polytechnic University, Hong Kong |
| Jinchi Lu | University of California, San Diego, USA |
| Xian-Zhang Ling | Qingdao University of Technology, China |
| Ahmed Elgamal | University of California, San Diego, USA |
| Arul K. Arulmoli | Earth Mechanics Inc., California, USA |